

©2022 Society of Photo-Optical Instrumentation Engineers (SPIE). One print or electronic copy may be made for personal use only. Systematic reproduction and distribution, duplication of any material in this paper for a fee or for commercial purposes, or modification of the content of the paper are prohibited.

Citation:

Janerra D. Allen, Sravani Varanasi, Elliot Hong, and Fow-Sen Choa "Flexible energy landscape analysis of functional connectivity through region bundling", Proc. SPIE 12122, Signal Processing, Sensor/Information Fusion, and Target Recognition XXXI, 1212215 (8 June 2022); <https://doi.org/10.1117/12.2619126>

DOI:

<https://doi.org/10.1117/12.2619126>

Access to this work was provided by the University of Maryland, Baltimore County (UMBC) ScholarWorks@UMBC digital repository on the Maryland Shared Open Access (MD-SOAR) platform.

**Please provide feedback**

Please support the ScholarWorks@UMBC repository by emailing [scholarworks-group@umbc.edu](mailto:scholarworks-group@umbc.edu) and telling us what having access to this work means to you and why it's important to you. Thank you.

# PROCEEDINGS OF SPIE

[SPIDigitalLibrary.org/conference-proceedings-of-spie](https://SPIDigitalLibrary.org/conference-proceedings-of-spie)

## Flexible energy landscape analysis of full brain functional connectivity through region bundling

Janerra Allen, Sravani Varanasi, Elliot Hong, Fow-Sen Choa

Janerra D. Allen, Sravani Varanasi, Elliot Hong, Fow-Sen Choa, "Flexible energy landscape analysis of full brain functional connectivity through region bundling," Proc. SPIE 12122, Signal Processing, Sensor/Information Fusion, and Target Recognition XXXI, 1212215 (8 June 2022); doi: 10.1117/12.2619126

**SPIE.**

Event: SPIE Defense + Commercial Sensing, 2022, Orlando, Florida, United States

# Flexible Energy Landscape Analysis of Full Brain Functional Connectivity through Region Bundling

Janerra D. Allen<sup>a</sup>, Sravani Varanasi<sup>b</sup>, Elliot Hong<sup>c</sup>, Fow-Sen Choa<sup>d\*</sup>

<sup>a, b, d</sup> University of Maryland, Baltimore County, 1000 Hilltop Circle, Baltimore MD 21250, USA

<sup>c</sup> University of Maryland, Baltimore, 620 West Lexington Street, Baltimore MD 21201, USA

## ABSTRACT

Segmenting the human brain into networks has been a useful approach in analyzing functional connectivity. Brain network bundling can determine which regions are engaged and if they are working together. The thalamus (THL) and basal ganglia (BSL) regions in the subcortical network are linked to multiple cortical areas due to their roles in neural circuitry outlined in the cortico-basal ganglia-thalamo cortical map. Here we explore their coupling with the default mode network (DMN), frontoparietal network (FPN), salience network (SAN), attention network (ATN), sensorimotor network (SSM), visual network (VIS), and auditory network (AUD) using the energy landscape technique. Energy landscape analysis helps identify the statistical differences in functional behaviors between the healthy control and patient groups, which are obtained from the fMRI activity time courses of the 9 internetworks. In this work, we focused on studying 107 schizophrenic patients and 86 healthy controls and obtained the constructed activity patterns and disconnectivity graphs of each subject. The differences between two groups are compared. The results from bundling THL and BSL with the DMN, FPN, SAN, ATN, SSM, VIS, and AUD shows that these regions are more strongly coupled in controls than in patients. After performing energy calculations and heat map generations, we observed several lower energy band states that are common among all control and patient subjects. The potential implications of these common band states are discussed.

**Keywords:** energy landscape analysis, fMRI, functional connectivity, biomarkers, bundling, schizophrenia

## 1. INTRODUCTION

### 1.1 Background

Approximately 2 million Americans have been diagnosed with schizophrenia to date. Schizophrenia is a long-term mental disorder involving cognitive, emotional, and behavioral changes, thus affecting how a person thinks, feels, and behaves [1], [2]. Some contributory factors are genetics, early environment, and neurobiology, in addition to psychological and social processes [2], [3]. Cognitive symptoms of schizophrenia include problems in attention, concentration, and memory [2], [4] [5]. Psychotic symptoms of schizophrenia include hallucinations, altered perceptions, and delusions which could result in loss of motivation, disinterest, or lack of enjoyment [3], [6]. Cognitive and psychotic impairments in schizophrenic patients are linked to specific patterns of cortico-subcortical connectivity that extend from the thalamus to the basal ganglia nuclei [7], [8]. The cortico-basal ganglia-thalamo cortical loop is a system of neural subcircuits, connecting the cortex, basal ganglia, and thalamus pathways to send information to and from the spinal cord [8]. The basal ganglia region is involved in brain processes that control movement, thoughts, and emotion, while the thalamus region relays sensory and motor signals to the cerebral cortex [9]. The 5 subcircuits (motor, oculomotor, dorsolateral prefrontal, lateral orbitofrontal, and anterior cingulate) allow the brain to complete complex tasks such as achieving goals and adapting to changing circumstances [10]. Difficulty completing such tasks could be attributed to cognitive and psychotic symptoms of schizophrenia as outlined.

---

\* Further author information: (Send correspondence to J.D.A.)

J.D.A: E-mail: [j178@umbc.edu](mailto:j178@umbc.edu), Telephone: 1 410 455 3272

S.V.: E-mail: [sravani1@umbc.edu](mailto:sravani1@umbc.edu), Telephone: 1 410 455 3272

\*This format was developed in 1995 by Rick Herman, SPIE, and Ken Hanson, Los Alamos National Laboratory

## 1.2 Brain Connectivity Using Energy Landscape Method

Energy landscape is an analysis tool used to calculate and interpret multivariate time series data, such as resting state-fMRI, and helps identify energy values at local minimums to understand the changes of between state transitions [11], [12]. Energy landscape analysis identifies statistical differences in functional behaviors between the healthy control and patient groups, which are obtained from the fMRI activity time courses of the internetworks. In this study, I investigated functional connectivity and brain activity differences between 107 schizophrenic (SZ) and 86 healthy normal control (HC) subjects using energy landscape analysis on resting-state functional magnetic resonance imaging (fMRI) data. For each subject, 9 connectivity networks, subcortical network (SUB) containing thalamus (THL) and basal ganglia (BSL), default mode network (DMN), frontoparietal network (FPN), salience network (SAN), attention network (ATN), sensorimotor network (SSM), visual network (VIS), and auditory network (AUD) were analyzed. The functional connectivity among the internetworks was evaluated using the time courses of the corresponding regions. A key motivation for functional network connectivity analysis between healthy controls and patients with schizophrenia, is to find biomarkers that would differentiate both groups. The differences in functional behavior between these groups could be attributed to internetwork activity. Potential biomarker differences between healthy controls and schizophrenic patients can be identified using the energy landscape analysis technique. Local minimums can become biomarkers if energy value differences are large enough. This paper discusses the role of flexibility and stability in brain states within coupled networks.

## 2. MATERIALS AND METHODS

### 2.1 Data Preprocessing

The resting-state data used for this study was collected by the Maryland Psychiatric Research Center at the University of Maryland School of Medicine. Of total participants in the study, 107 were HC and 86 were SZ. The MRI data were collected on a GE 1.5T scanner with an eight-channel head coil. Resting-state fMRI data were recorded with an EPI sequence. Each participant was instructed to relax with their eyes open for approximately 8 minutes, while the EPI data were recorded. These EPI data were preprocessed with SPM12/SPM8.

### 2.2 Brainnetome

The Brainnetome Atlas is a connectivity-based parcellation framework that contains information on anatomical and functional connections of 246 voxels or subregions [13]. We used 3D coordinates and subnetwork affiliations from the 264 region of interest (ROI) Power atlas and 90 ROI Automated Anatomical Labeling (AAL) atlas respectively, as a model to align the 246 voxels to 9 brain networks [11]. The Energy Landscape toolbox interpreted brain activity of internetwork connections among the 9 networks, including: THL, BSL, DMN, FPN, SAN, ATN, SSM, VIS, and AUD. This was interpreted based on the properties and functions of each brain region and subsequent brain network.

### 2.3 Energy Landscape

The energy landscape toolbox interpreted brain activity using the pairwise maximum entropy method (MEM) estimation [11], [12]. The pairwise MEM model is fitted to analyze probability distributions and energy values of the states generated. This was interpreted based on the properties and functions of each brain region and subsequent network. The energy landscape is achieved by 1) binarization of the data, 2) MEM from Boltzmann distribution calculating energy, likelihood, and maximum likelihood functions as seen in [11, eqs. (1), (2), (3), and (4)], 3) disconnectivity graph and basin of energy local minimum, and 4) dynamics of energy landscapes [11], [12]. We constructed activity patterns and disconnectivity graphs for each subgroup, SZ and HC, using the energy landscape toolbox to interpret the multivariate resting-state fMRI data.

Table 1: Subnetwork affiliations parceled into internetwork and intra-network connectivity.

| Number | Network | Gyrus                              | Architecture  |
|--------|---------|------------------------------------|---|
| 9      | SUB     | Thalamus                           | <i>left &amp; right</i> , medial prefrontal thalamus<br><i>left &amp; right</i> , pre-motor thalamus<br><i>left &amp; right</i> , sensory thalamus<br><i>left &amp; right</i> , rostral temporal thalamus<br><i>left &amp; right</i> , posterior parietal thalamus<br><i>left &amp; right</i> , occipital thalamus<br><i>left &amp; right</i> , caudal temporal thalamus<br><i>left &amp; right</i> , lateral prefrontal thalamus |
| 8      |         | Basal Ganglia                      | <i>left &amp; right</i> , ventral caudate<br><i>left &amp; right</i> , globus pallidus<br><i>left &amp; right</i> , nucleus accumbens<br><i>left &amp; right</i> , ventromedial putamen<br><i>left &amp; right</i> , dorsal caudate<br><i>left &amp; right</i> , dorsolateral putamen   |
| 7      | DMN     | Superior Frontal Gyrus             | <i>gyrus</i>  |
|        |         | Middle Frontal Gyrus               | <i>gyrus</i>  |
|        |         | Superior Temporal Gyrus            | <i>gyrus</i>  |
|        |         | Middle Temporal Gyrus              | <i>gyrus</i>  |
|        |         | Parahippocampal Gyrus              | <i>gyrus</i>  |
|        |         | Inferior Parietal Lobule           | <i>gyrus</i>  |
|        |         | Precuneus                          | <i>gyrus</i>  |
|        |         | Cingulate Gyrus                    | <i>gyrus</i>  |
| 6      | FPN     | Middle Frontal Gyrus               | <i>left &amp; right</i> , inferior frontal junction<br><i>left &amp; right</i> , ventral area 9/46<br><i>left &amp; right</i> , lateral area 10   |
|        |         | Inferior Frontal Gyrus             | <i>left &amp; right</i> , dorsal area 44<br><i>left &amp; right</i> , inferior frontal sulcus   |
|        |         | Inferior Parietal Lobule           | <i>left &amp; right</i> , rostradorsal areas 39 & 40<br><i>left &amp; right</i> , caudal area 40  |
| 5      | SAN     | Middle Frontal Gyrus               | <i>left &amp; right</i> , area 46   |
|        |         | Inferior Frontal Gyrus             | <i>left &amp; right</i> , caudal area 45<br><i>left &amp; right</i> , (opercular and ventral) area 44   |
|        |         | Insular Gyrus                      | <i>left &amp; right</i> , ventral agranular insula<br><i>left &amp; right</i> , dorsal agranular insula<br><i>left &amp; right</i> , dorsal granular insula   |
|        |         | Cingulate Gyrus                    | <i>left &amp; right</i> , pregenual area 32<br><i>left &amp; right</i> , caudodorsal area 24  |
| 4      | ATN     | Middle Frontal Gyrus               | <i>left &amp; right</i> , ventrolateral area 6  |
|        |         | Inferior Frontal Gyrus             | <i>left &amp; right</i> , rostral area 45   |
|        |         | Superior Temporal Gyrus            | <i>left &amp; right</i> , area 41/42  |
|        |         | Middle Temporal Gyrus              | <i>left &amp; right</i> , dorsolateral area 37  |
| 3      | SSM     | Superior Frontal Gyrus             | <i>gyrus</i>  |
|        |         | Precentral Gyrus                   | <i>gyrus</i>  |
|        |         | Paracentral Lobule                 | <i>gyrus</i> ,  |
|        |         | Superior Parietal Lobule           | <i>gyrus</i>  |
|        |         | Postcentral Gyrus                  | <i>gyrus</i>  |
|        |         | Cingulate Gyrus                    | <i>gyrus</i>  |
| 2      | VIS     | Fusiform Gyrus                     | <i>left &amp; right</i> , rostroventral area 20<br><i>left &amp; right</i> , medioventral & lateroventral area 37   |
|        |         | Medio Ventral Occipital Cortex     | <i>left &amp; right</i> , rostral & caudal lingual gyrus<br><i>left &amp; right</i> , rostral & caudal cuneus gyrus<br><i>left &amp; right</i> , ventromedial parietooccipital sulcus   |
|        |         | Lateral Occipital Cortex           | <i>left &amp; right</i> , middle & inferior occipital gyrus<br><i>left &amp; right</i> , area V5/MT+<br><i>left &amp; right</i> , occipital polar cortex<br><i>left &amp; right</i> , medial & lateral superior occipital gyrus   |
| 1      | AUD     | Superior Temporal Gyrus            | <i>left &amp; right</i> , TE1.0 & TE1.2<br><i>left &amp; right</i> , caudal area 22   |
|        |         | posterior Superior Temporal Sulcus | <i>left &amp; right</i> , rostro pSTS<br><i>left &amp; right</i> , caudo pSTS   |

The Boltzmann distribution is denoted by

$$P(\sigma | \mathbf{h}, \mathbf{J}) = \frac{\exp[-E(\sigma | \mathbf{h}, \mathbf{J})]}{\sum_{\sigma'} \exp[-E(\sigma' | \mathbf{h}, \mathbf{J})]} \quad (1)$$

with Energy,  $E$

$$E(\sigma | \mathbf{h}, \mathbf{J}) = \sum_{i=1}^N h_i \sigma_i - \frac{1}{2} \sum_{i=1}^N \sum_{j=1, j \neq i}^N J_{ij} \sigma_i \sigma_j \quad (2)$$

and maximum likelihood

$$(\mathbf{h}, \mathbf{J}) = \arg \max_{\mathbf{h}, \mathbf{J}} \mathcal{L}(\mathbf{h}, \mathbf{J}) \quad (3)$$

with likelihood,  $\mathcal{L}(\mathbf{h}, \mathbf{J})$

$$\mathcal{L}(\mathbf{h}, \mathbf{J}) = \prod_{t=1}^{t_{max}} P(\sigma(t) | \mathbf{h}, \mathbf{J}) \quad (4)$$

## 2.4 Local Minima

The local minimum are states that have lower energy (more frequent) states relative to their neighboring nodes,  $N$ . For every  $N$  ROIs, there are  $2^N$  possible connectivity states. In this study we are using 9 networks, so the total number of possible connectivity states becomes  $2^9 = 512$ . Two minimums are in different sets if the highest energy transitions state (a local maximum) or lowest energy pathway between them exceeds energy,  $E$  [11]. The local minimums represent connectivity states that are visited more frequently compared to their neighboring states. The local minimums which form the deeper basins in the energy landscape, have lower energy values and more stability. The number of local energy minimum (attractor states) is estimated and the disconnectivity graph shows the positions of the local minimum states and their relationships [11]. The numbers on the x-axis of the activity patterns and disconnectivity graphs labeling the energy local minimum states are consistently used in both panels. White and black cells represent variables (ROIs) that are active (+1) and inactive (-1), respectively. Local minimums were identified as potential biomarkers between patients and controls.

## 3. RESULTS AND DISCUSSION

The following results are taken along the internetwork regions. Each network was averaged in accordance with the Brainnetome cortical and subcortical region allocation. After obtaining the constructed activity patterns and disconnectivity graphs for SZ and HC, we generated heat maps based on the energy calculations. We observed energy band states for both subgroups.

### 3.1 Local Minima as Potential Biomarkers

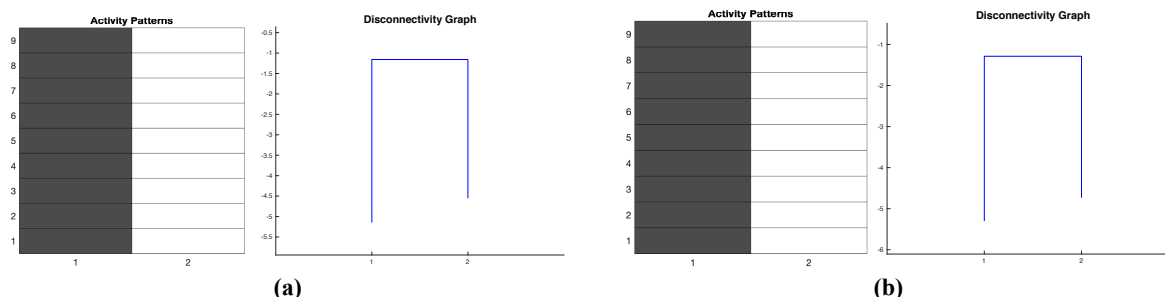


Fig. 1: Activity patterns and disconnectivity graphs for 7 internetworks of (a) all the averaged patients (b) all the averaged controls.

3.2 Energy Heatmaps for all Possible Connectivity States

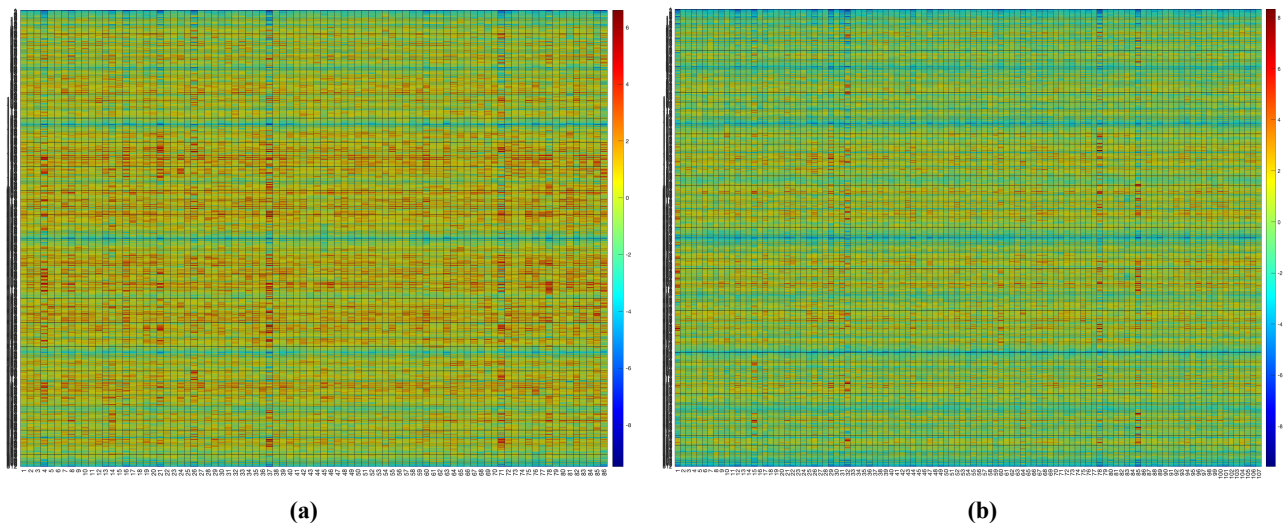


Fig. 2: Heatmaps of 9 internetwork ROIs for all 512 possible connectivity states per subgroup (a) 86 patients and (b) 107 controls. The y-axis represents connectivity states, and the x-axis represents each subject.

| BANDS        | 1  |    |    | 2  |    |    | 3   |     |     | 4   |     |     | 5   |     |     |     | 6   |     |     | 7   |     |     | 8   |     |     | 9   |     |     |
|--------------|----|----|----|----|----|----|-----|-----|-----|-----|-----|-----|-----|-----|-----|-----|-----|-----|-----|-----|-----|-----|-----|-----|-----|-----|-----|-----|
| STATE NUMBER | 1  | 2  | 3  | 65 | 66 | 67 | 129 | 130 | 131 | 191 | 192 | 193 | 255 | 256 | 257 | 258 | 320 | 321 | 322 | 382 | 383 | 384 | 446 | 447 | 448 | 510 | 511 | 512 |
| THL          | -1 | -1 | -1 | -1 | -1 | -1 | -1  | -1  | -1  | -1  | -1  | -1  | -1  | -1  | 1   | 1   | 1   | 1   | 1   | 1   | 1   | 1   | 1   | 1   | 1   | 1   | 1   | 1   |
| BSL          | -1 | -1 | -1 | -1 | -1 | -1 | 1   | 1   | 1   | 1   | 1   | 1   | 1   | 1   | -1  | -1  | -1  | -1  | -1  | -1  | -1  | -1  | 1   | 1   | 1   | 1   | 1   | 1   |
| DMN          | -1 | -1 | -1 | 1  | 1  | 1  | -1  | -1  | -1  | -1  | -1  | 1   | 1   | 1   | -1  | -1  | -1  | -1  | 1   | 1   | 1   | 1   | -1  | -1  | -1  | 1   | 1   | 1   |
| FPN          | -1 | -1 | -1 | -1 | -1 | -1 | -1  | -1  | -1  | 1   | 1   | -1  | 1   | 1   | -1  | -1  | 1   | -1  | -1  | 1   | 1   | 1   | 1   | 1   | 1   | 1   | 1   | 1   |
| SAN          | -1 | -1 | -1 | -1 | -1 | -1 | -1  | -1  | -1  | 1   | 1   | -1  | 1   | 1   | -1  | -1  | 1   | -1  | -1  | 1   | 1   | 1   | 1   | 1   | 1   | 1   | 1   | 1   |
| ATN          | -1 | -1 | -1 | -1 | -1 | -1 | -1  | -1  | -1  | 1   | 1   | -1  | 1   | 1   | -1  | -1  | 1   | -1  | -1  | 1   | 1   | 1   | 1   | 1   | 1   | 1   | 1   | 1   |
| SSM          | -1 | -1 | -1 | -1 | -1 | -1 | -1  | -1  | -1  | 1   | 1   | -1  | 1   | 1   | -1  | -1  | 1   | -1  | -1  | 1   | 1   | 1   | 1   | 1   | 1   | 1   | 1   | 1   |
| VIS          | -1 | -1 | 1  | -1 | -1 | 1  | -1  | -1  | 1   | 1   | 1   | -1  | 1   | 1   | -1  | -1  | 1   | -1  | -1  | -1  | 1   | 1   | -1  | 1   | 1   | -1  | 1   | 1   |
| AUD          | -1 | 1  | -1 | -1 | 1  | -1 | -1  | 1   | -1  | -1  | 1   | -1  | -1  | 1   | -1  | 1   | 1   | -1  | 1   | 1   | -1  | 1   | 1   | -1  | 1   | 1   | -1  | 1   |

Fig. 3: A total of 9 common bands along with their respective connectivity states for the 9 internetworks were identified for both patients and controls. The color coding represents the complementary connectivity pairs between groups, starting with the outermost state to the innermost state. Bands 1 and 9 show complementary pairs with state definitions 1 to 3 and 510 to 512, respectively. Bands 2 and 8 show complementary pairs with state definitions 65 to 67 and 446 to 448, respectively. Bands 3 and 7 show complementary pairs with state definitions 129 to 131 and 382 to 384, respectively. Bands 4 and 6 show complementary pairs with state definitions 191 to 193 and 382 to 384, respectively. Lastly, complementary pairs are shown within band 5 with state definitions 255 to 256 and 257 to 258.

3.3 Connectivity States and Complementary State Pairs

We used the subnetwork affiliations from the Power atlas and AAL atlas as models to bundle the 9 networks (THL, BSL, DMN, FPN, SAN, ATN, SSM, VIS, and AUD). This information was interpreted based on the properties and functions of each region. The activity patterns in Fig. 1 show that the 9 networks are activated together, thus correlated for both subgroups. The disconnectivity graphs in Fig. 1 reveal that SZ have slightly higher energy values, suggesting SZ have higher transitions between states. The all black and all white states shown for SZ have higher energy, meaning these regions' connections are not as strong as HC. We found that observing the heatmaps would provide more information about the underlying connectivity differences between SZ and HC. In Fig. 2, the energy values at each possible connectivity state were plotted as heatmaps and compared for both subgroups further revealing that the SZ have higher energy values than the HC. The heatmap results in Fig. 2 show that the HC map has more lower states than the SZ map, suggesting that the bands of

these lowest states are less distinct. A total of 9 common bands were identified for both patients and controls, as shown in Fig. 3. The bands identified as the following: band 1 with connectivity state numbers 1-3, band 2 with connectivity state numbers 65 to 67, band 3 with connectivity state numbers 129 to 131, band 4 with connectivity state numbers 191 to 193, band 5 with connectivity state numbers 255 to 258, band 6 with connectivity state numbers 382 to 384, band 7 with connectivity state numbers 382 to 384, band 8 with connectivity state numbers 446 to 448, and band 9 with connectivity state numbers 510 to 512. The low energy states do not change significantly, thus the connectivity between states change gradually. Like the white and black cells which represent the respective active (+1) and inactive (−1) ROIs, the connectivity states in Fig. 3 follows the same active and inactive definition. The color coding shown in Fig. 3 represents the complementary connectivity pairs and more likely to be the stable connectivity states among the total 512 connectivity states. A complementary pair is a connectivity state that is aligned with another connectivity state such that the ROIs are oppositely active and/or inactive. Hence the complementary pairs shown in bands 1 and 9 have state definitions of 1 to 3 and 510 to 512, respectively. Starting with the outermost state to the innermost state, connectivity state 1 is complementary to connectivity state 512, connectivity state 2 is complementary to connectivity state 511, and connectivity state 3 is complementary to connectivity state 510. Similarly, bands 2 and 8 show complementary pairs with state definitions 65 to 67 and 446 to 448, respectively. Connectivity state 65 is complementary to connectivity state 448, connectivity state 66 is complementary to connectivity state 447, and connectivity state 67 is complementary to connectivity state 446. Bands 3 and 7 show complementary pairs with state definitions 129 to 131 and 382 to 384, respectively. Connectivity state 129 is complementary to connectivity state 384, connectivity state 130 is complementary to connectivity state 383, and connectivity state 131 is complementary to connectivity state 382. Additionally, bands 4 and 6 show complementary pairs with state definitions 191 to 193 and 382 to 384, respectively. Connectivity state 191 is complementary to connectivity state 322, connectivity state 192 is complementary to connectivity state 321, and connectivity state 193 is complementary to connectivity state 320. Lastly, complementary pairs are shown within band 5 with state definitions 255 to 256 and 257 to 258. Connectivity state 255 is complementary to connectivity state 258 and connectivity state 256 is complementary to connectivity state 257. We can see that FPN, SAN, ATN, and SSM are consistently activated together, revealing the correlation between networks. The DMN and a combination of FPN, SAN, ATN, take turns controlling the VIS, AUD, SSM. In terms of common bands, the BSL and THL seem to be working independently with all cases. In Fig. 3 we can also see that the THL and BSL are either active or inactive together for specific bands and their respective complementary state pairs. THL and BSL are inactivated together in bands 1 and 2 containing states 1 to 3 and 65 to 67, respectively. While THL and BSL are activated together in bands 9 and 8 containing states 510 to 512 and 446 to 448, respectively. THL and BSL are also shown not working together and that only one is active at a time. THL and BSL are anticorrelated in bands 3, 4, 5, 6, and 7 containing states 129 to 131, 191 to 193, 255 to 258, 320 to 322, and 382 to 384, respectively.

#### 4. CONCLUSION AND FUTURE WORKS

In this study, we investigated functional connectivity and brain activity differences between 107 SZ and 86 HC subjects using energy landscape analysis on resting-state fMRI data. After collecting the energy values for each possible connectivity state, we evaluated the functional connectivity among the 9 internetworks. The activity patterns show that the 9 networks are activated together, thus correlated for both subgroups. The disconnectivity graphs reveal that SZ have slightly higher energy values, suggesting SZ have higher transitions between states. The all black and all white states shown for SZ had higher energy, meaning these regions' connections are not as strong as HC. These plots did not reveal enough information about the connectivity differences between SZ and HC, so we compared energy values using heatmap illustrations. The heatmaps revealed common band structures between both SZ and HC. The heatmap results show that the HC map appears bluer than the SZ map, suggesting that the bands of lowest states are less distinct.

Not only did we identify complementary state pairs which may help to form stable brain states, but we also noticed that FPN, SAN, ATN, and SSM are consistently activated or inactivated together, revealing the



correlation between these networks. The DMN and a combination of FPN, SAN, ATN, took turns controlling the VIS, AUD, SSM. For the common bands, the BSL and THL seem to be working independently with all cases. Additionally, THL and BSL were either active or inactive together for specific bands and their respective complementary state pairs. THL and BSL were also shown not working together other bands and their respective complementary state pairs. In these cases, only one is active at a time. This suggests that cortico-thalamic and cortico-basal ganglia connectivity of the brain networks were consistent across subcortical nuclei. Our future works include calculating the statistical differences between both subgroups and identifying the correlations between AUD and SSM which contribute to psychotic symptoms and correlations between SAL and THL which contribute to impaired cognition.

## ACKNOWLEDGMENTS

This research was supported by the University of Maryland, Baltimore County and University of Maryland, Baltimore. I am thankful to my colleagues Sravani Varanasi, Dr. Elliot Hong and Dr. Fow-Sen Choa who provided expertise that greatly assisted the research.

## REFERENCES

- [1] F. J. Charlson, et al., "Global Epidemiology and burden of schizophrenia: Findings from the global burden of disease study 2016," *Schizophrenia Bulletin*, vol. 44, no. 6, pp. 1195–1203, 2018.
- [2] K. R. Patel, J. Cherian, K. Gohil, and D. Atkinson, "Schizophrenia: overview and treatment options," *a peer-reviewed journal for formulary management*, vol. 39, no. 9, p. 638-45, 2014.
- [3] M. J. Owen, A. Sawa, and P. B. Mortensen, "Schizophrenia," *The Lancet*, vol. 388, no. 10039, pp. 86–97, 2016.
- [4] E. Antonova, T. Sharma, R. Morris, and V. Kumari, "The relationship between brain structure and neurocognition in schizophrenia: A selective review," *Schizophrenia Research*, vol. 70, no. 2-3, pp. 117–145, 2004.
- [5] B. T. Talreja, L. Kataria, and S. Shah, "Cognitive function in schizophrenia and its association with socio-demographics factors," *Industrial Psychiatry Journal*, vol. 22, no. 1, p. 47, 2013.
- [6] R. A. McCutcheon, T. Reis Marques, and O. D. Howes, "Schizophrenia—an overview," *JAMA Psychiatry*, vol. 77, no. 2, p. 201, 2020.
- [7] M. Avram, F. Brandl, J. Bäuml, and C. Sorg, "Cortico-thalamic hypo- and hyperconnectivity extend consistently to basal ganglia in schizophrenia," *Neuropsychopharmacology*, vol. 43, no. 11, pp. 2239–2248, 2018.
- [8] N. N. Foster et al., "The mouse cortico–basal ganglia–thalamic network," *Nature*, vol. 598, no. 7879, pp. 188–194, 2021.
- [9] M. E. D.-T. Herrero, C. Barcia, and J. Navarro, "Functional anatomy of thalamus and basal ganglia," *Child's Nervous System*, vol. 18, no. 8, pp. 386–404, 2002.
- [10] M. DeLong and T. Wichmann, "Changing views of basal ganglia circuits and circuit disorders," *Clinical EEG and Neuroscience*, vol. 41, no. 2, pp. 61–67, 2010.
- [11] T. Watanabe et al., "Energy landscapes of resting-state brain networks," *Frontiers in Neuroinformatics*, vol. 8, 2014.
- [12] T. Ezaki, T. Watanabe, M. Ohzeki, and N. Masuda, "Energy landscape analysis of neuroimaging data," *Philosophical Transactions of the Royal Society A: Mathematical, Physical and Engineering Sciences*, vol. 375, no. 2096, p. 20160287, 2017.
- [13] L. Fan et al., "The human Brainnetome Atlas: A new brain atlas based on Connectional Architecture," *Cerebral Cortex*, vol. 26, no. 8, pp. 3508–3526, 2016.